Mid-infrared study of stones from the Sutter's Mill meteorite

Michel NUEVO[1,2], Scott A. SANDFORD[1*], George J. FLYNN[3], and Susan WIRICK[4]

[1]NASA Ames Research Center, MS 245-6, Moffett Field, California 94035, USA
[2]SETI Institute, 189 N. Bernardo Ave., Suite 100, Mountain View, California 94043, USA
[3]Department of Physics, SUNY-Plattsburgh, 101 Broad St., Plattsburgh, New York 12901, USA
[4]Center for Advanced Radiation Sources, University of Chicago, 5801 S. Ellis Ave., Chicago, Illinois 60637, USA
[*]Corresponding author. E-mail: Scott.A.Sandford@nasa.gov

Abstract–The Sutter's Mill meteorite fell in northern California on April 22, 2012. Several fragments of the meteorite were recovered, some of them shortly after the fall, others several days later after a heavy rainstorm. In this work, we analyzed several samples of four fragments—SM2, SM12, SM20, and SM30—from the Sutter's Mill meteorite with two infrared (IR) microscopes operating in the 4000–650 cm^{-1} (2.5–15.4 μm) range. Spectra show absorption features associated with minerals such as olivines, phyllosilicates, carbonates, and possibly pyroxenes, as well as organics. Spectra of specific minerals vary from one particle to another within a given stone, and even within a single particle, indicating a nonuniform mineral composition. Infrared features associated with aliphatic CH_2 and CH_3 groups associated with organics are also seen in several spectra. However, the presence of organics in the samples studied is not clear because these features overlap with carbonate overtone bands. Finally, other samples collected within days after the rainstorm show evidence for bacterial terrestrial contamination, which indicates how quickly meteorites can be contaminated on such small scales.

INTRODUCTION

On April 22, 2012 at 14:51 UTC, a daytime fireball and sonic boom were observed by witnesses over California and Nevada. Following an air burst, the KBBX, KDAX, and KRGX weather radar detected fragments of the meteorite falling near the small townships of Coloma and Lotus in El Dorado County, California (Jenniskens et al. 2012). Some of these stones were collected at Sutter's Mill, at the historic site where the California gold rush was initiated, giving its name to the meteorite. The first three fragments of the Sutter's Mill carbonaceous chondrite were first recovered on April 24, before search efforts were complicated by a heavy 2-day rainstorm. At the time of publication of Jenniskens et al. (2012), a total of 77 pieces of the meteorite had been collected, for a total mass of 943 g, with the biggest stone weighing 205 g, and new stones continue to be found.

Preliminary analysis of some of the Sutter's Mill meteorite stones showed a cosmic-ray exposure age of 0.051 ± 0.006 Myr, consistent with a CM2 chondrite, and an age of 0.10 ± 0.04 Myr, measured from its ^{26}Al activity (Jenniskens et al. 2012). The origin of the parent body of Sutter's Mill is still debated, its projected orbit being in agreement with a Main Belt asteroid or a Jupiter-family comet (Jenniskens et al. 2012).

Mineralogy studies of Sutter's Mill classify it as a regolith breccia, and boundaries between distinct lithologies can be seen in some individual stones. Sutter's Mill shows similarities to CM chondrites and has been officially classified as a CM chondrite on the basis of its whole-rock chemistry and isotopic compositions of O, Os, and Cr (Jenniskens et al. 2012). However, Sutter's Mill also shows properties that distinguish it among the CM chondrites. For example, it has the lowest N/C and δ^{15}N ratios observed among CM2 chondrites, suggesting a different N-bearing organic composition. C and N isotopic ratios vary widely from one stone to another, which suggests the presence of two distinct organic phases, namely, a

Table 1. Information of the four stones from the Sutter's Mill meteorite studied in this work (from Jenniskens et al. 2012).

Stone	Mass (g)	Date collected	GPS coordinates	Finder(s)	Rained on	Microscope used
SM2	4.0	April 24, 2012	38.8029°N 120.9086°W	P. Jenniskens	No	Stand-alone
SM12	17.5	April 27, 2012	38.7857°N 120.9091°W	M. Waiblinger	Yes	Stand-alone
SM20	1.1	April 27, 2012	38.7857°N 120.9091°W	R. Garcia	Yes	Synchrotron
SM30	3.5	May 1, 2012	38.7989°N 120.8810°W	J. Matin M. Dayton	Yes	Synchrotron

volatile-rich and a volatile-poor component (Jenniskens et al. 2012).

This work presents a Fourier-transform infrared (FTIR) spectroscopy study in the mid-infrared (4000–650 cm^{-1}, 2.5–15.4 μm) range of small fragments from four stones of the Sutter's Mill meteorite, namely SM2 (4.0 g), SM12 (17.5 g), SM20 (1.1 g), and SM30 (3.5 g). SM2 and SM12 were analyzed with a stand-alone FTIR microscope, while SM20 and SM30 were independently analyzed with an FTIR microscope coupled to a synchrotron beam source. The results obtained from both techniques are compared to assess how sample compositions may vary within each stone and from one stone to another, and interpreted within the context of the mineral and organic composition of the Sutter's Mill meteorite. Finally, we try to estimate how the composition of these stones may have been affected by rain water, as most available stones of the Sutter's Mill meteorite, including three of the four we analyzed, were exposed to heavy rainfall for several days before they were collected.

SAMPLE SELECTION, PREPARATION, AND ANALYSIS

Sample Selection and Preparation

The samples analyzed in this work are small fragments from four stones of the Sutter's Mill meteorite (Table 1). SM2 was found in a parking lot and was the only sample studied in this work that was collected before the rainstorm, although it had unmistakably been run over by a car while in the parking lot. We received only a small amount of this fragment, and much of this material subsequently proved to contain fusion crust, although some nonfusion crust material could be analyzed. SM12, SM20, and SM30 fragments were collected after the rainstorm, so that they were probably exposed to water and terrestrial biological contamination. We had enough material from SM12 to select among available

fragments under a microscope, so we could reliably obtain samples of both fusion crust and nonfusion crust materials. Finally, we obtained milligram-mass samples from the SM20 and SM30 fragments, none of them showing any visible evidence for fusion crust.

Samples examined with the stand-alone FTIR microscope (SM2 and SM12), including both inner material of the meteorite and fusion crust, were deposited on a clean, gold-coated glass slide, crushed with a stainless steel roller tool, and placed directly on the focal plane of the microscope. Samples for analysis with the synchrotron-based microscope (SM20 and SM30) were each prepared by crushing a small piece (<1 mm in size) between two clean glass slides, and by tapping the slides to remove large particles. The meteoritic material that remained on the glass slide was suspended in a 600-μL sterilized water droplet (Sigma, No. W3500), and a copper TEM grid backed with silicon monoxide was used to collect material from the surface and near the surface of the droplet. The grid was then allowed to dry. Nonsoluble particles were randomly distributed over the whole TEM grid. This technique biases against large crystals and disperses small particles, generally less than a few μm in size, on the TEM substrate.

Infrared Analyses of the Samples

Stand-alone FTIR Microscope

Infrared spectra of fragments from the SM2 and SM12 samples were recorded with a Nicolet iN10 MX FTIR microscope in the mid-infrared range (4000–650 cm^{-1}, 2.5–15.4 μm), referred to as the molecular fingerprint region because many mineral and organic functional groups exhibit characteristic absorption features in that range. This microscope uses a convention globar light source and a liquid N$_2$-cooled MCT detector, and is capable of analyzing samples down to about 10 μm in size. IR spectra were collected by averaging 128 scans at a 4-cm^{-1} resolution in "reflection mode" using the spectrometer's OMNIC

software. In this mode, incoming IR photons pass through the samples, are reflected off the gold-coated substrate, and pass through the samples again on their way to the detector. Consequently, the IR data obtained are transmission spectra. Finally, for one fragment of stone SM12, an entire crushed 150-μm size particle was analyzed by recording IR spectra as a mosaic of overlapping 20-μm size windows with a spectral resolution of 4 cm^{-1}, to assess the variation of IR features as a function of the position on the grain.

Synchrotron-based FTIR Microscope

Samples from the SM20 and SM30 fragments were analyzed with synchrotron-based FTIR spectroscopy in the same 4000–650 cm^{-1} range as used with the stand-alone microscope. IR spectra were collected using a Nicolet Continuum microscope equipped with an MCT detector by averaging 1000 or 2000 scans at a 4-cm^{-1} resolution in transmission mode. This microscope is coupled to a synchrotron-generated IR beam on beamline U2b of the National Synchrotron Light Source (Brookhaven National Laboratory, Upton, New York, USA), which produces a highly polarized infrared beam that has ~1000 times the infrared intensity of a conventional globar source, providing a signal-to-noise ratio about 400 times better than conventional globar FTIR instruments. Such a high IR intensity allowed us to detect much weaker features than those accessible with other conventional instruments, and to operate with analysis beamspots much smaller than instruments equipped with globar sources. By operating close to the diffraction limit, with beamspots ranging from 7 μm × 7 μm to 10 μm × 10 μm, we were able to examine the dispersed Sutter's Mill samples at a spatial resolution that frequently provided spectra of isolated areas dominated by a single mineral and to investigate the types and abundances of organic matter associated with each mineral phase.

RESULTS AND DISCUSSION

Mineral Composition

Infrared spectra of the nonfusion crust material from fragments of all the Sutter's Mill stones examined in this work show compositions that are dominated by silicates or carbonates, or mixtures of both, although there is evidence for the presence of organic materials in some spectra (see Organic Materials section). Each of these components is addressed separately below.

Silicates

The nature of the observed silicate absorption features varied among the samples, the main silicate minerals observed being olivines and phyllosilicates, with some evidence for pyroxenes, all of them previously reported in several Sutter's Mill stones (Jenniskens et al. 2012). With the smaller beamspot sizes available to the synchrotron-based IR spectroscopy studies of samples SM20 and SM30, it was possible to obtain spectra from particles dominated by single mineral phases.

Phyllosilicates, identified on the basis of the dominant Si–O stretching feature consisting of a fairly symmetric, broad band centered near 1000 cm^{-1} (Sandford 1984, 1985), were relatively common in the Sutter's Mill samples (Fig. 1; Table 2). Some of the phyllosilicate spectra showed several O–H stretching mode bands (1) a narrow, weak feature centered near 3680–3650 cm^{-1}, due to water bound directly to cations in phyllosilicates (Bishop et al. 1994) and (2) a broader band around 3415–3350 cm^{-1}, due to adsorbed interlayer water. Many spectra also contain an H–O–H bending mode band near 1650 cm^{-1}. However, some phyllosilicate spectra did not display any water features, as shown in a few spots of SM30 (three middle traces of Fig. 1).

It is also interesting to note that many of the spectra in Fig. 1 show unusually large intensities of the H–O–H bend near 1650 cm^{-1} relative to the O–H stretch near 3300 cm^{-1}. This could potentially be the result of preterrestrial heating of the meteorite, whose orbit took it within less than 0.5 AU of the sun (Jenniskens et al. 2012). Sandford (1985) showed that stepwise-heating of a Murchison sample to above 1200 °C resulted in the decrease of the O–H stretching band relative to the H–O–H bending band, presumably because heating more easily removes adsorbed H_2O than structural O–H.

As three of the stones we examined—SM12, SM20, and SM30—were exposed to rain water, it is difficult to know how much of the water seen in their spectra (independent of dominant mineral in the spectrum), if any, is original to the meteorite. However, small amounts of phyllosilicates are present in some of our spectra of SM2, which was not exposed to rain, and these materials show clear bands of both adsorbed H_2O and structural O–H, suggesting that at least some water is probably associated with the original meteorite (see also Carbonates section and Fig. 3).

Spectra containing the Si–O stretching band of phyllosilicates often also contain features in the 1500–1400 cm^{-1} range due to carbonates, and features between 3000 and 2850 cm^{-1} that may be due to C–H stretching of aliphatic –CH$_3$ and –CH$_2$– groups, although these features may also be associated with carbonates, as discussed below. These features are generally much stronger in spectra dominated by
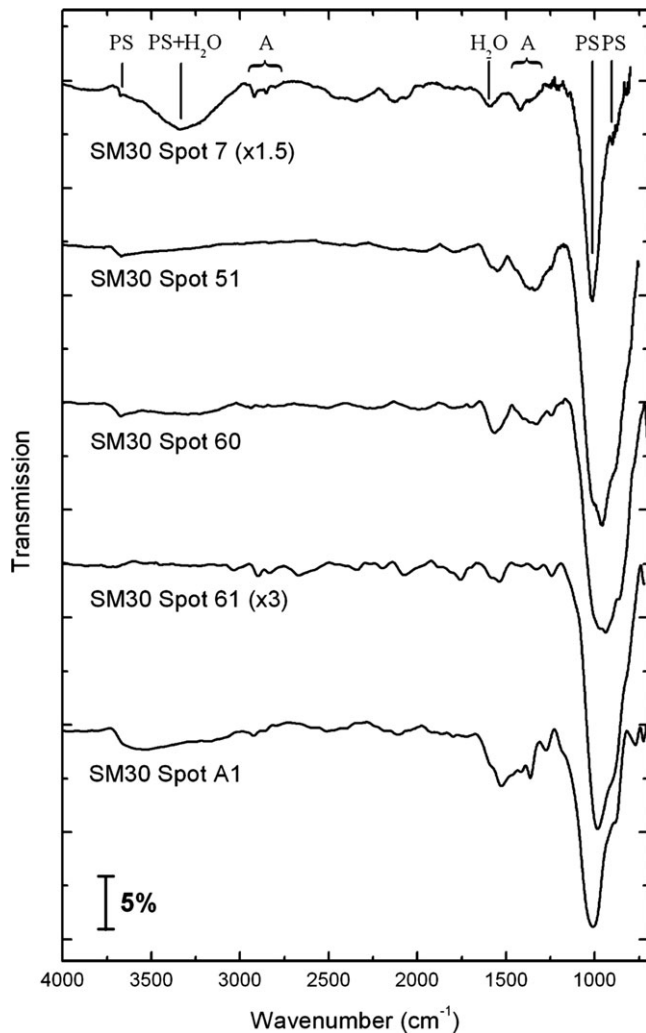
Fig. 1. Infrared spectra (4000–700 cm^{-1}) of five spots from SM30 showing the broad absorption of phyllosilicates near 1000 cm^{-1} (PS). Some spectra show O–H stretching mode bands, including a narrow, weak feature centered near 3680–3650 cm^{-1} due to water bound to phyllosilicates (PS), and a broader band around 3415–3350 cm^{-1}, due to adsorbed interlayer water, as well as an H–O–H bending mode band near 1650 cm^{-1} (H$_2$O). Many of the spectra also show features between 3000 and 2850 cm^{-1} that may be due to CH$_3$/CH$_2$ stretching modes (A), together with their bending modes in the 1455–1395 cm^{-1} range (A). Carbonates may also be present in a few samples such as SM30 spot A1 (bottom trace).

Fig. 2. Infrared spectra (4000–650 cm^{-1}) of three ~10 μm × 10 μm spots from SM20 containing olivine as indicated by the characteristic absorption bands near 1000 and 880 cm^{-1} (O). The top spectrum shows the characteristic profile of the pure olivine Si–O stretching band. The lower two spectra show different profiles for the olivine feature near 1000 cm^{-1}, which could be due to the polarization of the IR beam used to take these spectra and/or the presence of phyllosilicates (PS). Weaker features in the 1650–1400 cm^{-1} range in the two lower spectra are not inconsistent with the presence of H$_2$O and carbonates (C) associated with phyllosilicates.

phyllosilicates than spectra dominated by other minerals.

Some of the grains we examined clearly contain abundant olivine. Figure 2 shows the spectra of three spots of the SM20 stone that show the characteristic pair of olivine Si–O stretching features centered near 1000 and 880 cm^{-1} (Table 2). The variation in t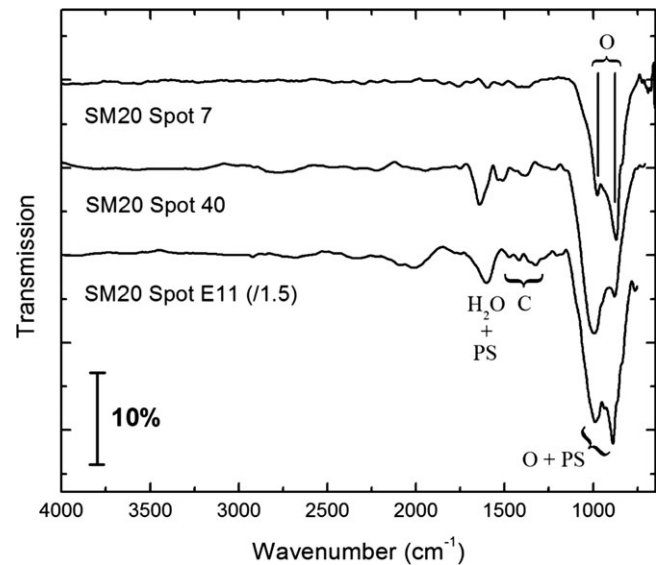he relative intensities of the two features probably results, in part, from different crystal orientations relative to the polarized infrared analysis beam, and suggests that each sample is dominated by either a single large crystal or multiple crystals all having similar orientations. The top spectrum (spot 7) shows a classic olivine silicate feature. The two bottom spectra (spots 40 and E11) show proportionally larger bands near 1000 cm^{-1} relative to the feature at 880 cm^{-1} and could also contain some contributions from phyllosilicates, as suggested by the presence of weak features in the 1650–1400 cm^{-1} range consistent with the presence of water and carbonates (Table 2). In all cases, the spots dominated by olivine exhibit only very weak, sometimes nondetectable, bands in the 3000 and 2850 cm^{-1} range associated with aliphatic C–H stretching absorption. Finally, as also observed in spectra dominated by phyllosilicates (Fig. 1), the spectra of spots 40 and E11 in Fig. 2 show unusually large intensities of the H–O–H bend near 1650 cm^{-1}, potentially due to preterrestrial heating of the meteorite.

Spectra of a few spots of the stones we examined are also consistent with the presence of pyroxenes, characterized by a strong Si–O absorption feature near 1100–1000 cm^{-1}. Olivines and phyllosilicates generally do not produce strong features above 1000 cm^{-1}.

Table 2. Identification of the bands observed in the infrared spectra of the Sutter's Mill meteoritic samples studied. Features labeled in the figures are those assigned to phyllosilicates (PS), aliphatic CH_3/CH_2 modes (A), carbonates (C), amides (AI and AII), olivines (O), and water (H_2O).

Position (cm^{-1})	Position (μm)	Identified species/groups	Nature of vibration
3680–3650	2.72–2.74	H_2O (phyllosilicate, bound)	O–H stretch
3420–3350	2.92–2.99	H_2O (phyllosilicate, interlayer)	O–H stretch
~3265	~3.06	H_2O	O–H stretch
~3065	~3.26	Aromatic CH	C–H stretch
2980–2870	3.36–3.48	Carbonate	Overtone ($2\nu_3$)
2980–2970	3.36–3.37	Aliphatic CH_3	CH_3 asymmetric stretch
2930–2925	3.41–3.42	Aliphatic CH_2	CH_2 asymmetric stretch
2875–2855	3.48–3.50	Aliphatic CH_3/CH_2 (blended)	CH_3/CH_2 symmetric stretch
~2515	~3.98	Carbonate	Overtone ($\nu_1 + \nu_3$)
~1795	~5.57	Carbonate	Overtone ($\nu_3 + \nu_4$)
1700–1600	5.88–6.25	Amide I	C=O stretch
~1650	~6.06	H_2O	H–O–H bend
~1650	~6.06	Aromatic C=C	C=C stretch
1600–1500	6.25–6.67	Amide II	N–H bend & C–N stretch
1500–1350 (broad)	6.67–7.14	Carbonate	CO_3 asymmetric stretch (ν_3)
1455–1395	6.87–7.17	Aliphatic CH_3/CH_2	C–H bend
1100–1000 (sharp)	9.09–10.00	Pyroxene	Si–O stretch
~1085	~9.22	Carbonate	CO_3 symmetric stretch (ν_1)
1010–990 (broad)	9.90–10.10	Phyllosilicate	Si–O stretch
~1000	~10.00	Olivine	Si–O stretch
~880 (sharp)	~11.36	Carbonate	CO_3 scissoring (ν_2)
~880	~11.36	Olivine	Si–O stretch
~715	~13.99	Carbonate	CO_3 asymmetric bend (ν_4)

However, the large range of spectral details allowed by the wide substitutional and structural ranges available for pyroxenes makes precise identification difficult.

Carbonates

Phyllosilicates were typically seen in association with carbonates in our spectra, and in many cases, the carbonate features dominate the spectra (Fig. 3). Carbonate minerals produce a number of characteristic IR absorption features (Jones and Jackson 1993) and are frequently seen in the spectra of CM carbonaceous chondrites (e.g., Sandford 1984) and interplanetary dust particles (IDPs) dominated by phyllosilicates (Sandford and Walker 1985; Sandford 1986). However, the abundance of carbonates in meteorites like Murchison is sufficiently small that often only the strongest, broad carbonate feature centered near 1450 cm^{-1} is seen in the spectra of "bulk" samples. In rare cases, for example the IDP "Calrissian," carbonates are abundant enough to display an additional narrow carbonate feature near 880 cm^{-1} (Sandford 1986).

Carbonates are common and abundant in our Sutter's Mill samples, although given the small size of our samples and the small scales on which we studied them, it is not clear how representative this is of the whole stones. Figure 4 shows five spots, three from the

SM20 stone and two from the SM30 stone, which are dominated by carbonates as indicated by the strong, broad absorption band centered near 1450 cm^{-1} and the weaker, sharp absorption band near 880 cm^{-1} (Table 2). Carbonates are also seen in SM2 (Fig. 3) and SM12 (Fig. 5). Variations of the positions of the carbonate bands indicate carbonates with different compositions, and possibly crystallographic structures, which are present in the Sutter's Mill meteorite.

As we were able to analyze very small samples, it was possible to obtain spectra of grains that consisted mostly of carbonates. This allowed us to detect weaker carbonate bands that are not normally observed in the spectra of larger meteoritic samples. For this purpose, one large (~150-μm diameter) particle from stone SM12 that was dominated by carbonates was crushed onto a glass slide and analyzed with the IR microscope by collecting a mosaic of 182 spectra covering the area of the whole dispersed particle.

Little variation was observed among these 182 spectra and the top trace in Fig. 5 shows the average spectrum of all these spectra. The strongest feature in the average spectrum is a broad band centered around 1455 cm^{-1} due to the ν_3 CO_3 asymmetric stretch vibrations and corresponds to the strongest carbonate feature seen in the spectra of many "bulk" CM chondrite
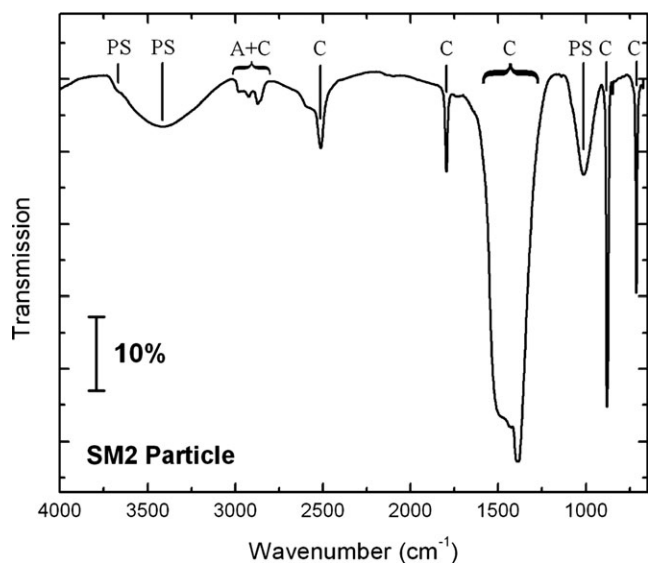
Fig. 3. Infrared spectrum (4000–650 cm^{-1}) of a fragment of SM2 showing absorption features associated with carbonates (C), phyllosilicates (PS), and a series of features in the 3000–2850 cm^{-1} range that can be due to aliphatic hydrocarbons (A), overtones of carbonate (C) bands, or a combination of both. The nature and symmetries of all these vibration modes are given in Table 2.

samples and IDPs dominated by phyllosilicates (Sandford 1984; Sandford and Walker 1985). This mode is doubly degenerate, and, under some conditions, may split into two distinct vibrations of different frequencies. In the spectra of "bulk" CM material, this band typically appears as a single, largely symmetric feature, but in the case of the carbonate particle discussed here, the band is clearly split into two distinct features centered at 1518 and 1387 cm^{-1} (Fig. 5, top trace). The averaged spectrum of this particle also shows additional carbonate fundamental vibrational features at 1083 cm^{-1} (v_1, CO_3 symmetric stretch), 879 cm^{-1} (v_2, CO_3 scissoring mode), and 711 cm^{-1} (v_4, CO_3 asymmetric bend) (Table 2). These fundamental vibrational features in this spectrum are strong enough that it is also possible to see additional features due to overtones and combinations of the fundamental bands (Fig. 5, top trace). Those weaker features are typically not seen in bulk CM spectra. The strongest of these fall near 2515 and 1796 cm^{-1}, and a weaker trio of bands is seen in the 2980–2870 cm^{-1} region, which is particularly problematic, as it nearly perfectly overlaps with the location of aliphatic C–H stretching modes and complicates the detection of organics in the samples (see below).

The four lower spectra shown in Fig. 5 correspond to different carbonate standards dispersed in KBr pellets and measured in transmission: aragonite (CaCO$_3$), calcite (CaCO$_3$), dolomite ((CaMg)(CO$_3$)$_2$), and siderite (FeCO$_3$). The composite spectrum of the
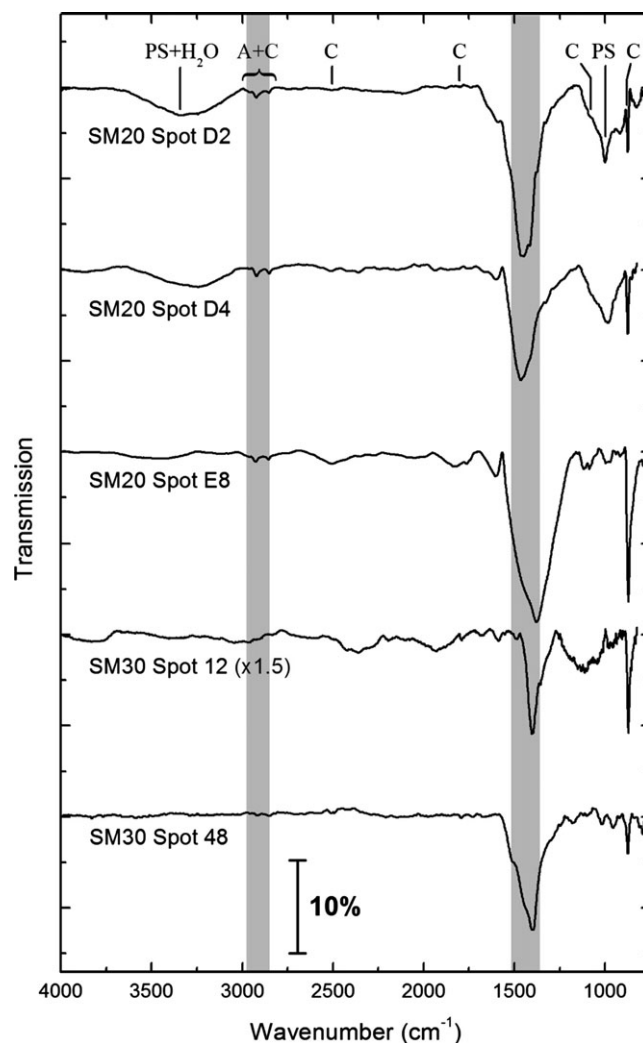

Fig. 4. Infrared spectra (4000–750 cm^{-1}) of five spots, three from SM20 and two from SM30, showing strong carbonate absorptions near 1450 cm^{-1} (marked with a vertical gray shaded band). The other vertical gray shaded area marks the 2v_3 overtone of the main carbonate (C) band, which produces bands between 3000 and 2850 cm^{-1} that can be confused with aliphatic CH$_3$/CH$_2$ groups (A). Carbonates also display a number of additional features (C). A few of these spectra also show phyllosilicate bands (PS), which are commonly associated with carbonates in our Sutter's Mill samples.

SM12 grain in Fig. 5 (top trace) does not match perfectly with any of the carbonates, although it shares general features with all of them and is not inconsistent with the spectra of calcite and dolomite, which have previously been identified in other Sutter's Mill stones with different analytical techniques (Jenniskens et al. 2012).

Finally, the individual spectra from carbonate-rich particles often also show weak bands characteristic of phyllosilicates that vary in intensity relative to the carbonate bands from spectrum to spectrum. For
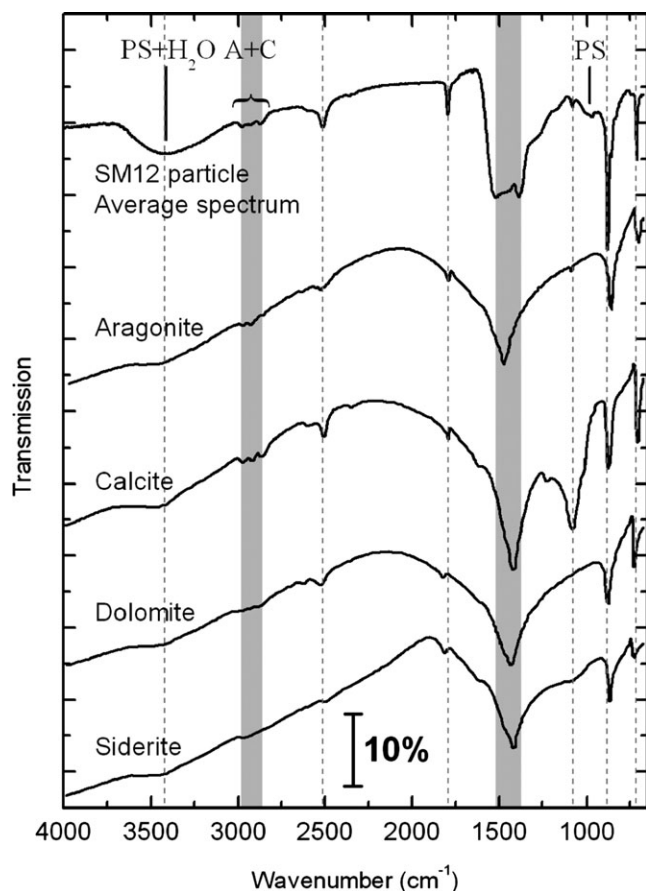
Fig. 5. Average infrared spectrum (4000–650 cm^{-1}) obtained by combining the 182 individual mosaic spectra of a ~150 μm grain from SM12 that consists largely of carbonates (top trace), and comparison with the infrared spectra of several carbonate standards: aragonite (CaCO$_3$), calcite (CaCO$_3$), dolomite ((CaMg)(CO$_3$)$_2$), and siderite (FeCO$_3$). Carbonate standard spectra are taken from Sandford (1985) and are from mineral standards prepared in KBr pellets, which cause the wavelength-dependent scattering losses observed at higher wavenumbers. The vertical gray shaded bands mark the locations of the strong ν_3 carbonate band and its overtone. Features in this overtone region in the spectrum of the SM12 particle may also contain contributions from the aliphatic CH$_3$/CH$_2$ stretching modes of organics (see text). Other carbonate bands are marked with vertical dashed lines. Weak phyllosilicate (PS) and H$_2$O features are also present.

example, the spectrum of the carbonate-rich particle shown in Fig. 3 contains an adsorbed H$_2$O band near 3420 cm^{-1}, a weak structural O–H band near 3680 cm^{-1}, and a weak Si–O stretching band near 990 cm^{-1}, all features typical of phyllosilicates (Table 2).

Organic Materials

A number of spectra from our samples show evidence for absorption bands in the 3050–2855 cm^{-1} region that are usually associated with C–H stretching

modes in organic materials. However, interpretation of these features being due solely to organics requires some caution, particularly for those samples whose spectra show evidence for abundant carbonates.

As noted above, carbonates can produce absorption features in the 2980–2870 cm^{-1} region that are due to overtones of the strong asymmetric CO$_3$ stretching mode near 1455 cm^{-1} (Figs. 3 and 5), and which seriously overlap with the asymmetric and symmetric stretching modes of aliphatic CH$_3$ and CH$_2$ groups. A good example of this issue is illustrated in Fig. 6, which compares the spectrum of the same carbonate grain from SM12 that is shown in Fig. 5 with those of three spots from the SM20 stone displaying strong features in the 3050–2855 cm^{-1} region and the calcite standard shown previously in Fig. 5. The full-range spectra of the SM12 particle, the three SM20 spots, and the calcite standard (Fig. 6a) are all dominated by features associated with carbonates, in particular the intense, broad band centered near 1455 cm^{-1} (Table 2). An enlargement of these spectra to the 3050–2800 cm^{-1} region (Fig. 6b) shows some variation in intensity and position for the bands associated with C–H stretching modes and/or carbonate overtones. The IR spectrum of the SM12 grain (top trace) displays three main features at 2981, 2928, and 2870 cm^{-1} whose positions and relative intensities are very similar to those of the calcite standard (bottom trace). The spectra of two SM20 spots (D2 and E7, top middle and middle traces, respectively) also display three main bands with very similar profiles, whose relative intensities are significantly different from those observed for the SM12 particle and calcite. Finally, the spectrum of SM20 spot 18 in this region (Fig. 6b, top middle trace) is unique and has features that resemble those usually associated with C–H stretching modes in aliphatic hydrocarbons, with the asymmetric modes (2990–2925 cm^{-1}) more intense than the symmetric modes (2900–2850 cm^{-1}). However, it is difficult to estimate how much of these bands results from the contribution of C–H stretching bands associated with organics, because the full-range spectra of these samples (Fig. 6a) are all clearly dominated by carbonate bands. Therefore, the identification of organics in general, and aliphatic hydrocarbons in particular, in meteoritic samples containing significant amounts of carbonates should be viewed very cautiously.

Although most of the potential organic matter observed in the sample spectra was associated with mineral grains, we identified rare areas dominated by organic matter, ranging up to several micrometers in size, in both SM20 and SM30 samples. Figure 7 shows that such organic-rich spots in both of these samples have essentially identical infrared spectra. These spectra look remarkably like the spectra of bacteria shown in
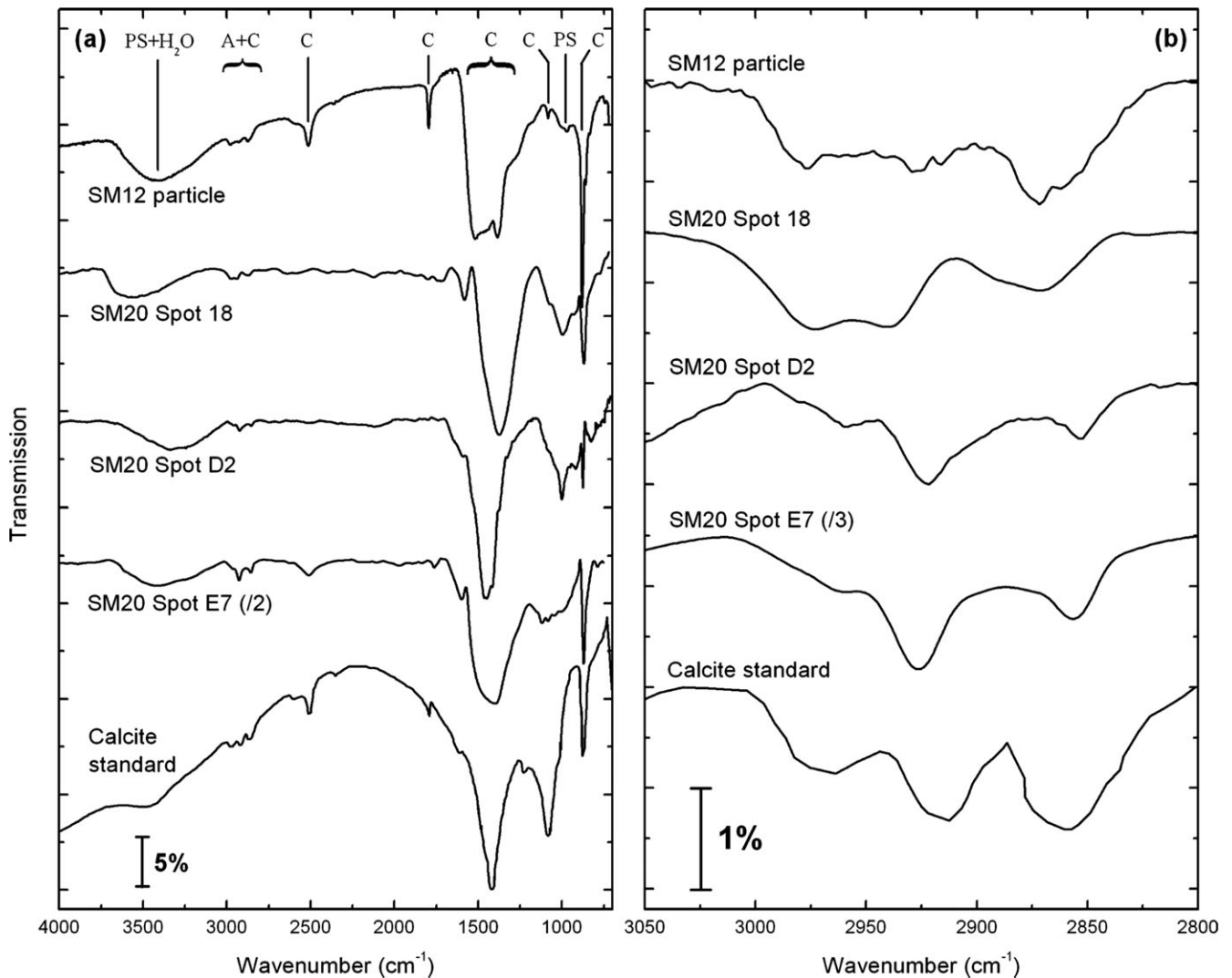
Fig. 6. a) Infrared spectra (4000–700 cm^{-1}) of three spots dominated by carbonates from SM20 (three middle traces), compared with the spectra of the SM12 carbonate particle (top trace) and a calcite standard (bottom trace). All those spectra show strong features characteristic of carbonates. b) The same five infrared spectra as in panel (a) in the CH$_3$/CH$_2$ stretching mode region (3050–2800 cm^{-1}). In this region, spectra were baseline-corrected to better compare the relative intensities of the features.

Igisu et al. (2009), suggesting that these spots are dominated by terrestrial contamination. In this regard, we note that the relative intensities of the C=O and C–H stretching bands in the spectra of Fig. 7 do not look like those typical of most IDPs and Murchison (Flynn et al. 2003). Given that these stones were exposed to rain for only a few days, they serve as cautionary tales of how quickly a meteorite can be contaminated on these size scales in the terrestrial environment.

Fusion Crust and Other Materials

The fusion crust on Sutter's Mill is unusually thick, and when plucked from the stones, often shows three gradated layers: an outer ablation zone, a sintered layer, and adhering inner materials. These layers are generally difficult to separate from one another. Samples of the fusion crust consisting of these combined three layers were analyzed from both stones SM2 and SM12, but the spectra provide little significant information about the original meteorite. IR spectra of fusion crust from SM12 (Fig. 8) appear much simpler than those measured for nonfusion crust materials. They are dominated by a strong unidentified silicate feature around 1000 cm^{-1}, and contain much weaker features associated with water, no bands associated with organics, as well as possible evidence for thermally altered carbonates.

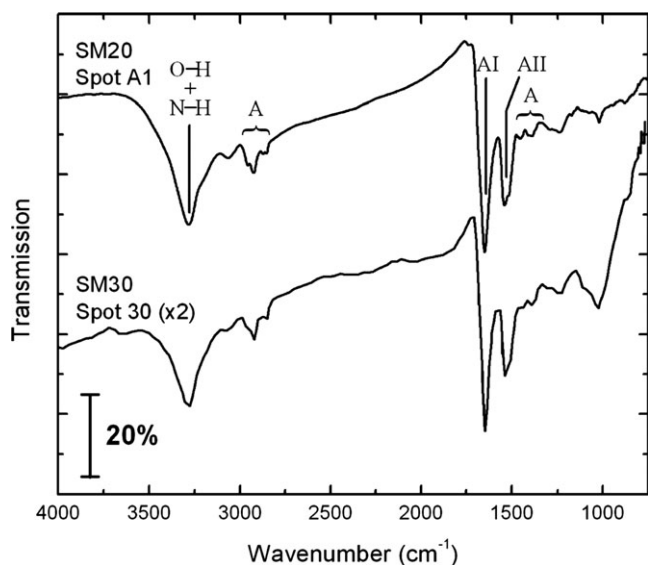The spectrum of one particle from the SM2 stone showed a complex IR spectrum (not shown) indicative

Fig. 7. Infrared absorption spectra (4000–750 cm^{-1}) of organic-rich spots in SM20 and SM30, showing a large number of features associated with O–H/N–H stretching modes, aliphatic C–H stretching modes (A), the C=O stretching mode from amide I (AI), the C–N–H stretching mode from amide II (AII), and the aliphatic C–H bending modes. These bands all strikingly resemble the IR spectra of bacteria (Igisu et al. 2009) and thus suggest that these Sutter's Mill samples have been biologically contaminated on micron-size scales.

of organics that was very different from previously observed normal meteoritic organics or meteoritic IOM. As SM2 was found in a parking lot where it had been broken into bits after being run over by a vehicle, and as most of the SM2 particles we received were dominated by fusion crust, we suspect this organic material to originate from a car tire. However, not having a sample of the offending tire, we could not verify this, so that the nature of the material from which this spectrum was obtained remains unresolved.

CONCLUSIONS

IR spectroscopy of the samples from the SM2, SM12, SM20, and SM30 stones from the Sutter's Mill meteorite show a number of absorption features associated with the presence of minerals, including phyllosilicates, olivines, pyroxenes, carbonates, as well as organics. Spectral details differ between different particles within a given stone, and even within a single particle, implying that the minerals are not uniform in composition. Carbonates are abundant in our samples and show a series of weaker carbonate bands not normally observed in the spectra of "bulk" CM chondrites. Overtones of the strongest carbonate band
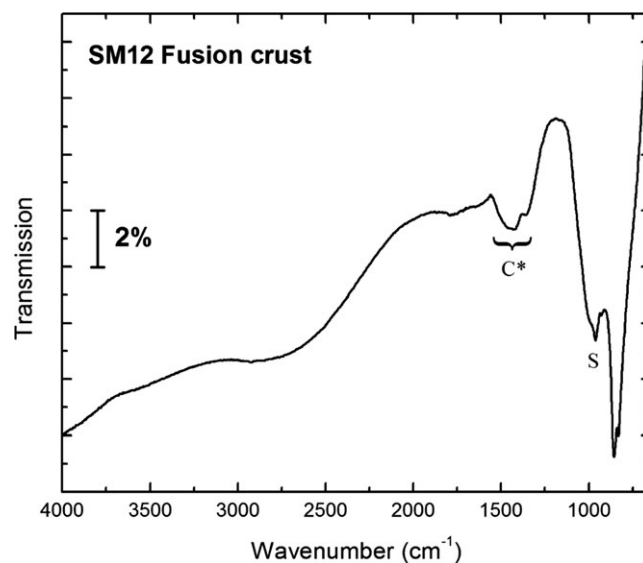

Fig. 8. Infrared spectrum (4000–650 cm^{-1}) of a sample of the fusion crust of stone SM12. Features on this spectrum could not be formally identified, although it may show the presence of unidentified silicates (S) near 1000 cm^{-1} as well as strongly altered carbonates (C*) near 1500–1350 cm^{-1}.

near 1455 cm^{-1} fall at the same location as aliphatic C–H stretching modes, so caution must be taken when interpreting aliphatic features in materials rich in carbonates. We see features at the spectral positions characteristic of aliphatic –CH_2– and –CH_3 features, but these are difficult to interpret when overlapping carbonate bands are present. Additional caution should be taken in interpreting the presence of organics in these samples, given that we see evidence for bacterial contamination even though those samples were collected within days of landing. Samples of SM2 may also contain possible contamination associated with the car tire that crushed the original stone.

REFERENCES

Bishop J. L., Pieters C. M., and Edwards J. O. 1994. Infrared spectroscopic analyses on the nature of water in montmorillonite. *Clays and Clay Minerals* 42:702–716.

Flynn G. J., Keller L. P., Feser M., Wirick S., and Jacobsen C. 2003. The origin of organic matter in the solar system: Evidence from the interplanetary dust particles. *Geochimica et Cosmochimica Acta* 67:4791–4806.

Igisu M., Ueno Y., Shimojima M., Nakashima S., Awramik S. M., Ohta H., and Maruyama S. 2009. Micro-FTIR spectroscopic signatures of bacterial lipids in proterozoic microfossils. *Precambrian Research* 173:19–26.

Jenniskens P., Fries M. D., Yin Q.-Z., Zolensky M., Krot A. N., Sandford S. A., Sears D., Beauford R., Ebel D. S., Friedrich J. M., Nagashima K., Wimpenny J., Yamakawa A., Nishiizumi K., Hamajima Y., Caffee M. W., Welten K. C., Laubenstein M., Davis A. M., Simon S. B., Heck P. R., Young E. D., Kohl I. E., Thiemens M. H., Nunn M. H., Mikouchi T., Hagiya K., Ohsumi K., Cahill T. A., Lawton J. A., Barnes D., Steele A., Rochette P., Verosub K. L., Gattacceca J., Cooper G., Glavin D. P., Burton A. S., Dworkin J. P., Elsila J. E., Pizzarello S., Ogliore R., Schmitt-Kopplin P., Harir M., Hertkorn N., Verchovsky A., Grady M., Nagao K., Okazaki R., Takechi H., Hiroi T., Smith K., Silber E. A., Brown P. G., Albers J., Klotz D., Hankey M., Matson R., Fries J. A., Walker R. J., Puchtel I., Lee C.-T. A., Erdman M. E., Eppich G. R., Roeske S., Gabelica Z., Lerche M., Nuevo M., Girten B., and Worden S. P. 2012. Radar-enabled recovery of the Sutter's Mill meteorite, a carbonaceous chondrite regolith breccia. *Science* 338:1583–1587.

Jones G. C. and Jackson B. 1993. *Infrared transmission spectra of carbonate minerals.* New York: Chapman & Hall.

Sandford S. A. 1984. Infrared transmission spectra from 2.5 to 25 microns of various meteorite classes. *Icarus* 60:115–126.

Sandford S. A. 1985. Laboratory infrared transmission spectra from 2.5 to 25 microns of individual interplanetary dust particles. Ph.D. thesis, Washington University, St. Louis, MO, USA.

Sandford S. A. 1986. Acid dissolution experiments—Carbonates and the 6.8-micrometer bands in interplanetary dust particles. *Science* 231:1540–1541.

Sandford S. A. and Walker R. M. 1985. Laboratory infrared transmission spectra of individual interplanetary dust particles from 2.5 to 25 microns. *The Astrophysical Journal* 291:838–851.